Chemical evidence for advection of interstitial fluid in the sedimentary series of the Barbados accretionary complex (Leg 110).

Barbados accretionary complex
Interstitial water
Chemical composition
Advection
Diagenesis

Prisme d'accrétion de la Barbade
Eau interstitielle
Composition chimique
Advection
Diagenèse

Gérard BLANC [a], **Jacques BOULÈGUE** [b], **Joris M. GIESKES** [c]

[a] Centre de Géochimie de la Surface (UPR 6251), Institut des Sciences de la Terre, Université Louis Pasteur, 1, rue de Blessig, 67084 Strasbourg Cedex, France.
[b] Laboratoire de Géochimie et Métallogenie, Université Pierre et Marie Curie, U.A. CNRS 196, 4, place Jussieu 75252 Paris, France.
[c] Ocean Research Division A-115, Scripps Institution of Oceanography, La Jolla, California 92093, USA.

Received 19/02/90, in revised form 14/06/90, accepted 19/06/90.

ABSTRACT

We report here our findings on the chemistry of methane, manganese and chloride dissolved in the interstitial water of the Barbados accretionary complex. The *décollement* separating the subduction plate from the accretionary wedge is geochemically characterized by high methane and manganese and low chloride concentrations relative to buried seawater. Sandstone layers occurring below the *décollement* and the compressive structures recording some of the earliest effects of offscraping are also characterized by similar anomalies. A fluid with the same characteristics is also found six kilometres to the east of the deformation front within the oceanic plate. High manganese concentration and low chlorinity also occur in the pore water of the offscraped sediment packages, but without associated anomalous methane concentrations.

These results suggest that:
- Dewatering processes occur below the *décollement* in association with thermogenic methane production;
- Fluid with low chlorinity and high methane concentrations circulates mainly along the *décollement*, its propagation in the oceanic domain and along the main fracture zones being associated with these detachment surfaces;
- Diagenetic processes essentially control the dissolved manganese concentration and probably affect the methane content of the interstitial waters;
- The observations made in this paper illustrate advective processes in the front of an accretionary prism.

Oceanologica Acta, 1991.**14**, 1, 33-49.

RÉSUMÉ

Mise en évidence de circulation de fluide dans le prisme d'accrétion de la Barbade (Leg 110).

Dans cet article sont rapportées les concentrations en méthane, manganèse et chlorure dissous dans les eaux interstitielles du prisme d'accrétion de la Barbade. Le décollement séparant les séries sédimentaires accrétées de celles plongeant en subduction, se caractérise par des concentrations élevées en méthane et manganèse mais faibles en chlorures par rapport à l'eau de mer. Les niveaux de sable rencontrés sous le décollement et les structures

0399-1784/91/01 33 17/$ 3.70/© Gauthier-Villars

en compression du front de déformation sont marqués par des anomalies similaires. Un fluide avec les mêmes caractéristiques a été également mis en évidence à 6 km en avant du front de déformation, dans le domaine océanique. De fortes concentrations en manganèse et de faibles chlorinités se trouvent dans les séries accrétées, mais ces anomalies ne sont pas associées avec des concentrations anormales en méthane.

Ces résultats suggèrent que :
• Des processus d'expulsion d'eau existent en-dessous du plan de décollement, en association avec une production de méthane thermogénique ;
• Du fluide caractérisé par une faible chlorinité et de fortes concentrations en méthane circule principalement le long du plan de décollement, de sa propagation dans le domaine océanique et le long des principaux accidents structuraux associés avec ces surfaces de détachement ;
• Les concentrations en manganèse dissous semblent essentiellement contrôlées par des processus diagénétiques impliquant probablement une consommation du méthane dissous par oxydation ;
• Les observations faites dans cet article illustrent la circulation d'un fluide au front d'un prisme d'accrétion.

Oceanologica Acta, 1991. **14**, 1, 33-49.

INTRODUCTION

The most important features of subduction zones are derived from their active tectonic situation. In this active zone, fluid flow in sediments plays a fundamental role in diagenesis and tectonic processes. That water flows out of an accretionary complex is known from direct observations (Boulègue *et al.*, 1987a) or by inference from the reduction of porosity of the sedimentary rocks that form them (von Huene and Lee, 1983; Bray and Karig, 1985; Kulm *et al.*, 1986).

It is generally assumed that most of the water flow is from pore water expelled from the underthrust and offscraped sedimentary series. This expulsion of fluid results from a progressive compaction in response to the increased load relative to the thickening of the upper series produced by the input of detrital sediments coming from the continent and by the especially pronounced tectonic stresses at the toe of an accretionary complex. However, dehydration reactions and meteoric waters coming from continental rainfall could also contribute to these hydrological processes acting at active continental margins.

Leg 110 of the Ocean Drilling Programme was specifically designed to investigate the relationship between structural, hydrological and diagenesis processes at the toe of an accretionary complex (Moore, Mascle *et al.*, 1987, 1988; Behrmann, Brown *et al.*, 1988; Blanc *et al.*, 1988).

The northern Barbados accretionary wedge (Fig. 1) became the focus of subduction zone drilling because the sedimentary cover of the incoming oceanic crust is less than 800 m thick and, consequently, the *décollement* and related thrust faults occur at relatively shallow depths below the sea-floor. Results from Deep Sea Drilling Project Leg 78A at the Barbados Ridge suggest that high fluid pressures are found along the *décollement* zone separating the underthrusting Atlantic Ocean crust and the overthrusting Caribbean plate, but drilling failed to penetrate this major fault surface (Biju-Duval, Moore *et al.*, 1984).

Leg 110 of ODP occupied six sites, 671 to 676, which comprised a transect of the toe of the northern Barbados accretionary wedge, about 23 km long. This transcet starts at 11 km up-slope and west of the deformation front, and stops at 6 km east of the deformation front in the oceanic domain (Fig. 1). The first penetration of the décollement zone separating two plates in a subduction area was achieved in the initial drilling location, Site 671 and then in Site 675.

In this article, we emphasize particularly significant results obtained from the methane, chloride, and manganese concentrations dissolved in the interstitial waters of the sediments of the Barbados accretionary complex in the Leg 110 work zone. We shall see below that these components can be considered as particularly revelant tracers of information about plausible processes of dewatering and fluid movement in an accretionary complex.

Sampling and analyses

Samples for geochemical studies were obtained in order to follow any changes with depth in interstitial water constituents in as much detail as possible.

Sediment sampling used for removal of interstitial water and gas analyses were simultaneously and immediately taken upon arrival of the cores on deck.

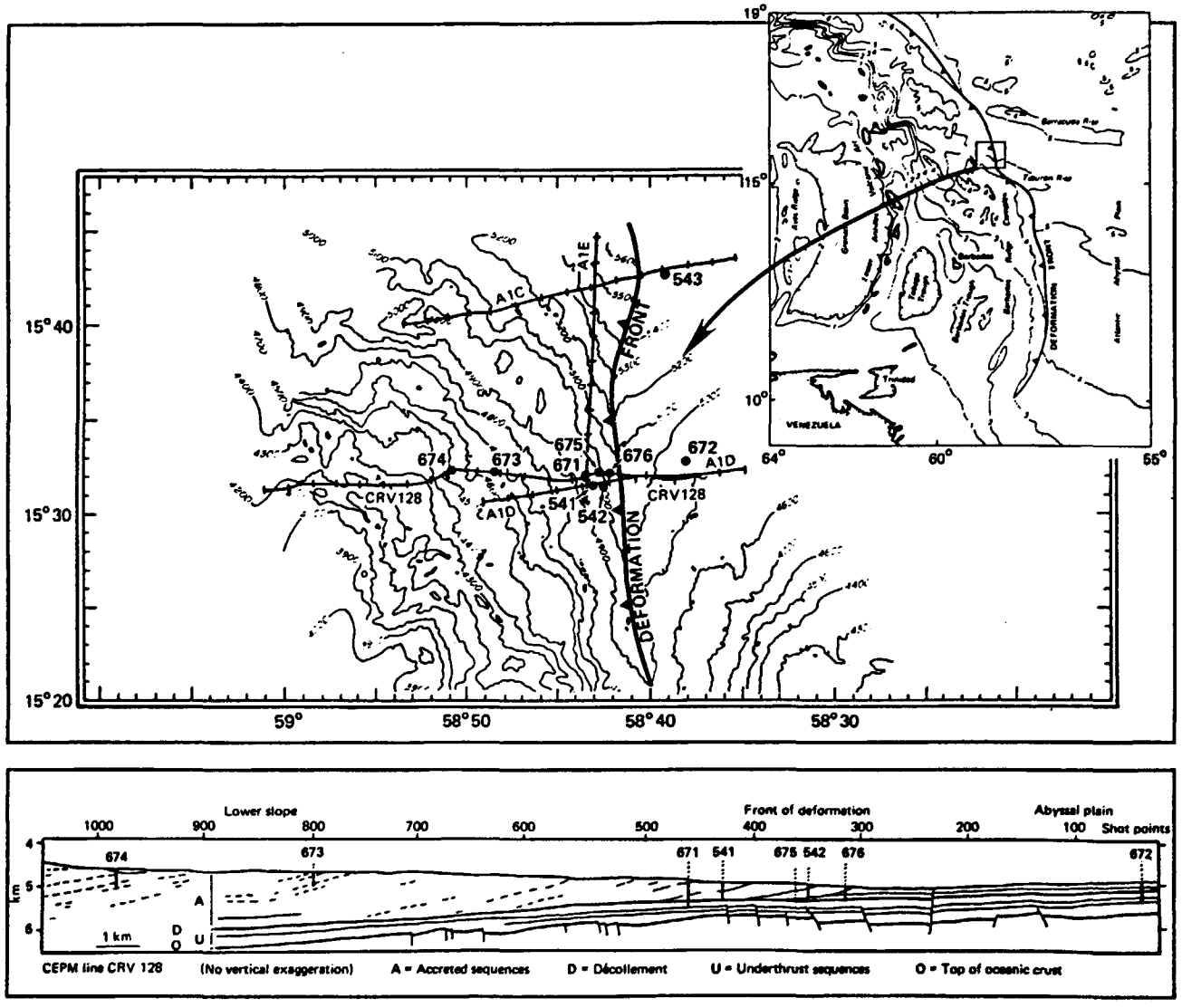

Figure 1

Top, the Seabeam bathymetric map shows the deformation front, drill sites of the Legs 78A and 110, and the seismic line used to locate sites. Bottom, Leg 110 sites are shown in this schematic depth section across the lower Barbados ridge accretionary complex.
En haut, Carte bathymétrique Seabeam montrant le front de déformation. Sites de forages des Legs 78A et 110 localisés sur le profil sismique CRV 128. En bas, la localisation des sites de forages du Leg 110 sont positionnés sur une coupe schématique de la zone étudiée du prisme d'accrétion de la Barbade.

Pore water squeezing

The method of obtaining interstitial waters from sediment using a stainless-steel press was described by Manhein (1966, 1974). Interstitial water was filtered through a 0.45 µm Millipore filter and collected in 50 cm^3 syringes.

Chloride

On board, chloride determinations with silver nitrate were carried out by means of potentiometric titration. The potential was measured with the electrode couple: Ag/Ag_2S. The Gran method was used to evaluate the equivalence volume (Jagner and Arén, 1970). Accurate results to within about 0.5 % of the IAPSO seawater standard were obtained with this method. The chloride concentrations are given in millimoles per litre (mM).

Manganese

The concentrations of dissolved manganese in interstitial water samples were analyzed by atomic absorption spectrometry in a Hitachi Z-7 000 spectrophotometer. This equipment accurately measures atomic absorption by the polarized Zeeman method while compensating for the background. This instrument is also equipped with an optical temperature controller able to provide atomization temperature, depending on the graphite cuvette emission's intensity. Use of such a control system increases the peak signal and improves the sensitivity. The background absorption interference caused by salt molecules could be minimized through the addition of a matrix modifier (Blanc and de Kersabiec, 1985; de Kersabiec *et al.*, 1985). The accuracy obtained with this method ranges from 2 to 5%. The results are expressed in micromoles per litre (µM).

Hydrocarbon gas

The sampling method for interstitial water dissolved methane analysis was recently improved during the Hydrotherm cruise to the Atlantis II deep (Blanc *et al.*, 1986; Blanc, 1987; Blanc *et al.*, 1990). A small volume of the headspace sediment sample was placed in a borosilicate glass vial; this vial was filled to approximately two-thirds of its total volume with sodium azide poisoned, hydrocarbon-free sea water. The sodium azide (NaN_3) inhibits any possible microbial activity after sampling. The vial was agitated on a high-speed shaker to partition gas into a helium-filled headspace similar to the method used by Bernard *et al.* (1976, 1978). The headspace methane was then analyzed by gas chromatography in a Hewlett-Packard 5890A coupled to an automatic Hewlett-Packard 19395a Headspace sampler. Methane concentrations are then expressed in micromoles per kilogram of interstitial water (µM), calculated from the sediment dry weight and original water content was given by physical property studies (Mascle, Moore *et al.*, 1988). The accuracy of the method is in the range of 5 % for a dissolved methane concentration of about 5 µM of interstitial water. All the methane concentrations determined on board and also the chloride and manganese concentrations are given in Table 1.

Table 1

Methane, chloride and manganese concentrations. Methane concentrations are expressed in micromoles per kilogram of interstitial water (µM), chloride in millimoles per litre (mM) and manganese in micromoles per litre (µM).
Concentrations en méthane, chlorure et manganese. Les concentrations en méthane sont exprimées en micromoles par kilogramme d'eau interstitielle (µM), les concentrations en chlorure et manganese en millimoles et micromoles par litre respectivement (mM et µM).

Data geochemistry Leg 110

Hole 671B

Core - Section	Depth (m)	CH_4 (µM)	Cl (mM)	Mn (µM)
1-3	4,5	19,1	559	97.9
2-5	16	n.d.	564	135
3-4	22	n.d.	570	77.7
4-5	33	n.d.	574	70.3
5-5	43	27,4	n.d.	n.d.
6-4	50,5	n.d.	570	51.9
8-5	68,5	n.d.	568	55.9
10-3	86	n.d.	571	52.2
13-3	113	23,5	559	95.0
14-6	125	n.d.	570	n.d.
15-1	127	5,2	572	n.d.
17-4	153	3,5	573	153
I.SS.	164	n.d.	567	58.7
19-1	171	12,9	569	52.8
22-5	200	28,5	570	63.0
25-4	230	7	570	48.1
28-5	260	26,5	564	16.4
31-1	290	n.d.	560	7.4
32-5	300	25,4	n.d.	n.d.
33-2	310	n.d.	554	n.d.
34-3	320	16,6	533	71.7
37-2	348	34,5	539	74.1
40-3	368	13,6	539	102
43-3	397	26,1	536	84.8
46-3	420	n.d.	526	95.6
48-5	442	15,1	n.d.	n.d.
49-3	450	15	551	162
50-3	458	286	n.d.	n.d.
51-4	470	258,2	n.d.	n.d.
52-2	477	151,8	520	204
55-5	508	550	505	535
56-2	516	n.d.	508	n.d.
58-6	535	n.d.	552	149
59-5	546	259	n.d.	n.d.
61-5	566	76,1	556	46.1
63-5	580	147	560	25.1
65-5	600	238,9	547	19.8
67-5	620	356,5	564	16.7
70-5	650	450,4	563	25.7
73-5	675	535	508	n.d.
74-1	685	n.d.	542	n.d.

Hole 675

Core - Section	Depth (m)	CH_4 (µM)	Cl (mM)	Mn (µM)
2-2	325	724	500	254
3-2	334	307	537	102
4-3	345	317	527	243
5-3	355	n.d.	531	265
6-5	366	394	512	517
8-4	385	396	541	487

Hole 672A

Core - Section	Depth (m)	CH_4 (µM)	Cl (mM)	Mn (µM)
1-4	6	22	560	n.d.
2-6	12	n.d.	563	158
3-4	18	n.d.	563	119
4-5	29	46	562	143
5-5	38.5	n.d.	563	91.0
I.S.1	40	n.d.	561	126
7-5	57.5	55	563	118
9-5	76	88	562	41.7
I.S.2	89	n.d.	564	39.3
12-5	105	99	562	90.8
15-3	130	n.d.	559	104
I.S.3	132	n.d.	550	61.0
18-3	158	119	552	92.3
21-2	185	n.d.	565	317
24-5	216	208	540	210
27-5	245	57	554	77.4
30-5	274	50	549	23.8
32-4	290	n.d.	549	21.1
34-4	309	100	573	26.9
36-4	327	93	532	38.8
38-5	346	114	518	80.6
39-2	352	n.d.	576	59.2
40-5	367	72	505	n.d.
41-1	376	69	n.d.	n.d.
42-2	382	37	522	n.d.
43-4	395	55	529	n.d.
46-1	424.5	168	n.d.	n.d.
46-1	425	n.d.	535	n.d.
48-3	447	101	527	111
51-2	470	136	545	134
53-3	489	126	572	150

Hole 673B

Core - Section	Depth (m)	CH_4 (µM)	Cl (mM)	Mn (µM)
1-4	6	<5	549	1.3
2-5	15	<5	559	75.5
3-5	24	<5	569	116
4-5	34	<5	563	84.6
5-4	42	<5	559	128
7-1	57	<5	555	99.7
9-3	79	<5	551	94.1
12-2	105	<5	549	74.6
15-5	136	<5	512	100
18-2	164	<5	513	91.4
22-2	200	<5	505	53
25-4	230	<5	541	n.d.
28-5	260	<5	543	522
31-6	290	<5	491	182
34-5	318	<5	548	444

Hole 674

Core - Section	Depth (m)	CH_4 (µM)	Cl (mM)	Mn (µM)
1-3	4.5	<5	546	2.0
2-6	15.5	<5	543	58.8
3-5	23.5	<5	537	137
4-3	30	<5	518	335
5-4	40.5	<5	569	201
7-2	57	<5	565	111
9-6	82	<5	553	93.2
12-3	105	<5	558	152
15-2	132	<5	543	135
18-5	165	<5	530	84.8
21-3	190	<5	527	75.9
24-5	220	<5	501	62.3
27-5	250	<5	481	n.d.
30-3	275	<5	508	41.3
33-5	308	<5	455	87.6
36-5	336	<5	465	154
39-5	365	<5	489	397
42-3	391	<5	455	298
45-4	421	<5	459	84.3
48-3	448	<5	394	63.9

Hole 676

Core - Section	Depth (m)	CH_4 (µM)	Cl (mM)	Mn (µM)
1-3	5	84	558	139
2-5	13	<5	561	175
3-5	22	<5	563	98.8
4-5	33	409	560	148
I.S.1	36	<5	562	n.d.
5-5	42	206	561	187
7-5	61	26	558	92.3
8-5	70	<5	563	87.5
I.S.2	73	<5	559	n.d.
10-5	89	<5	559	73.2
I.S.3	92	<5	530	n.d.
12-2	105	<5	560	63.3
15-2	133	<5	558	61.5
17-5	155	<5	554	87.2
19-5	170	<5	549	108
21-5	190	293	547	114
23-4	210	<5	544	122
25-1	228	<5	543	108
27-5	250	<5	519	163
28-6	260	<5	536	250
30-5	275	<5	547	544
31-3	286	150	537	528
32-3	295	<5	546	541
33-5	305	<5	548	382

On board, we were unable to determine the light hydrocarbon C_2 and C_3 contents because the detection limit of the flame ionization detector was not low enough to measure these species. Therefore, for some double samples collected in Hole 676, some $C_1/(C_2+C_3)$ ratios were determined by the Marine Geology Laboratory of the Centre de Brest (IFREMER).

Carbonate carbon and X-ray diffraction analyses

These determinations were performed on dry-powdered sediments sampled at the same levels as those used for the chemical interstitial water studies. Carbonate carbon was determined on board by means of the Coulometrics 5030 Carbonate Carbon apparatus. With this apparatus, about 250 mg of dried, powdered sediment was gently heated and reacted with HCl. The resulting CO_2 was transferred to a coulometer with ethanolamine as the indicator solution. The CO_2 was converted to a strong acid and the changing colour of the solution was monitored with respect to a standard sample. For each sample, the percentage of calcium carbonate was calculated from the inorganic content. Semi-quantitative mineralogical determinations were also performed on board by means of X-ray diffractometry with an internal mineralogical standard. The plot of the calcite percentage versus the percentage of calcium carbonate determined from the inorganic carbon analysis yields a quite linear function with a correlation coefficient of about 0,965 (Fig. 2).
This result can be used to consider the semi-quantitative mineralogical determinations as a representative distribution of the variability rates of the four major mineralogical components (total clays, quartz, plagioclase, calcite) occurring in the cored sediments. Both X-ray and inorganic carbon data are given in Table 2.

RESULTS

Site 671

The Hole 671 penetrated about 500 m of Pleistocene to lower Miocene imbricately thrusted, offscraped calcareous mud and mudstone, a 40 m thick *décollement* zone with scaly mudstone and 150 m of little deformed underthrust Oligocene mudstone, marlstone, and siltstone.
The X-ray semi-quantitative mineralogical determinations indicate that the variability with depth of the amounts of calcite, total clay, quartz and plagioclase minerals is in good agreement with the lithological observations (Fig. 3). Indeed, calcite occurs from the mudline to 360 mbsf, then below clays become the most abundant minerals. The occasional enrichments of plagiocalse may probably be related to occurrences of ash layers.

The *décollement* zone at Site 671 is tectonically defined only by a strongly developed zone of scaly fabric extending from 500 to 540 mbsf. No major biostratigraphic inversion or large increase of porosity was noticed. The host beds of the *décollement* zone at this site are lower Miocene to upper Oligocene radiolarian-bearing brown to olive-gray claytones.

The concentration-depth profiles of dissolved methane, chloride and manganese in the interstitial waters in the Hole 671 sedimentary series are given in Figure 3.

The concentration-depth profile of dissolved methane shows low and fairly uniform values from the mudline to 450 mbsf. The amount of methane is fairly constant,

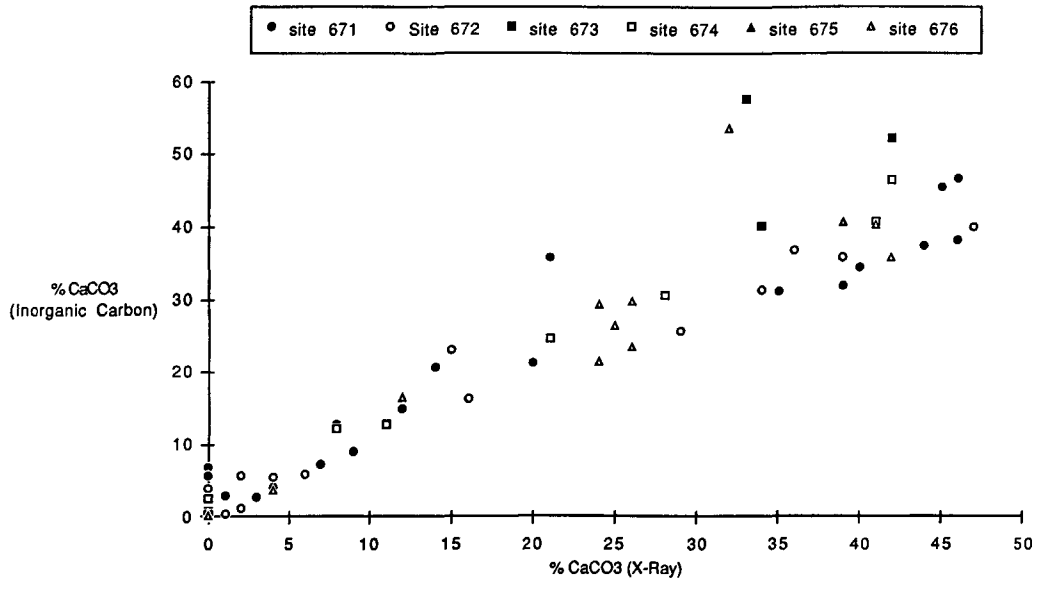

Figure 2

Diagram of the percentage of calcium carbonate versus percentage of calcite.
Diagramme des pourcentages en carbonate de calcium en fonction des pourcentages de calcite.

Table 2

Total clay, quartz, plagioclase and calcite percentage (%) determined by means of X-ray diffractometry analyses. Inorganic carbon contents (IC (%)) determined by means of coulometric analyses, calcium carbonate percentages ($CaCO_3$ (%)) determined from inorganic carbon data.
Pourcentages (%) en calcite, quartz, plagioclase et argiles déterminés par diffractométrie des rayons X sur diagramme de poudre. Contenus en carbone inorganique (IC (%)) déterminés en colorimétrie. Pourcentages en $CaCO_3$ (%) déterminés à partir des données de carbone inorganique.

HOLE 671B							
core-section	Depth (m)	Total clay (%)	Quartz (%)	Plagio. (%)	Calcite (%)	CaCO3 (%)	IC (%)
1-3	4.5	61	9	18	12	15,08	1.81
2-5	16	43	11	42	4	4,09	0.49
3-4	22	35	17	13	35	31,16	3,74
4-5	33	33	14	13	40	34,5	4,14
6-4	50.5	63	11	12	14	20,6	2,47
8-4	68.5	43	12	6	30	32,08	3,85
10-3	86	59	7	13	21	35,92	4,31
13-3	113	72	16	9	3	2,83	0,34
17-4	153	69	15	9	7	7,25	0,87
19-1	171	29	15	10	46	38,42	4,61
22-5	200	45	11	0	44	37,58	4,51
25-4	230	55	9	15	21	24,83	2,98
28-5	260	39	11	5	45	45,58	5,47
31-1	290	42	10	2	46	46,91	5,63
34-3	320	57	10	13	20	21,41	2,57
37-2	348	75	8	9	8	12,75	1,53
40-3	368	90	6	4	0	6,99	0,84
43-3	397	88	7	5	0	0,08	0,01
46-3	420	88	7	4	1	2,99	0,36
49-3	450	86	11	3	0	0,17	0,02
52-2	477	93	0	7	0	0,33	0,04
55-5	508	80	8	12	0	0,08	0,01
58-6	535	78	21	1	0	0,17	0,02
61-5	566	83	14	3	0	0,17	0,02
63-5	580	62	27	2	9	9	0,99
65-5	600	81	19	0	0	0,17	0,02
67-5	620	86	14	0	0	0,67	0,08
70-5	650	81	19	0	0	5,67	0,68
73-5	675	84	16	0	0	0,17	0,02
HOLE 672							
1-4	6	49	9	6	36	36,9	4,43
2-6	12	28	7	63	2	1,17	0,14
3-4	18	44	14	8	34	31,4	3,77
4-5	29	52	16	16	16	16,41	1,97
5-5	38,5	34	13	6	47	40,1	4,82
7-5	57,5	48	11	2	39	36	4,43
12-5	105	81	7	7	5	9	2,78
15-3	130	86	8	6	0	23,1	0,01
18-3	158	85	2	13	0	0,08	0,08
21-2	185	70	13	17	0	0,49	0,02
24-5	216	97	0	3	0	0,17	0,02
27-5	245	90	9	1	0	0,17	0,02
30-5	274	90	9	1	0	0,33	0,04
32-4	290	77	22	0	1	0,44	0,09
36-4	327	95	2	3	0	0,58	0,07
38-5	346	15	85	0	0	0,41	0,05
39-2	352	98	2	0	0	3,9	0,48
40-5	367	93	4	3	0	0,41	0,05
41-1	376	96	4	0	0	0,92	0,11
42-2	382	53	18	0	29	25,7	3,09
43-4	395	75	19	0	6	5,9	0,71
46-1	424,5	16	83	0	0	--	--
46-1	425	97	0	3	0	0,25	0,03
48-3	447	90	6	0	4	5,6	0,67
51-2	470	92	6	0	2	5,8	0,7
53-4	489	88	12	0	0	0,24	0,03

HOLE 673							
core-section	Depth (m)	Total clay (%)	Quartz (%)	Plagio. (%)	Calcite (%)	CaCO3 (%)	IC (%)
1-4	6	78	7	15	0	0,17	0,02
2-5	15	47	9	2	42	52,38	6,28
3-5	24	38	10	18	34	40,37	4,84
4-5	34	36	10	21	33	57,7	4,52
5-4	42	81	5	14	0	0,75	0,09
7-1	57	70	9	21	0	0,25	0,03
9-3	79	81	8	11	0	0,33	0,04
12-2	105	81	7	12	0	0,42	0,05
15-5	136	81	4	15	0	0,5	0,06
18-2	164	93	2	5	0	0,5	0,06
22-2	200	83	9	8	0	0,66	0,08
25-4	230	89	4	7	0	0,42	0,05
28-5	260	88	8	4	0	0,17	0,02
31-6	290	84	10	6	0	0,42	0,05
34-5	318	82	8	10	0	0,17	0,05
HOLE 674							
1-3	4,5	51	9	32	8	12,18	1,46
2-6	15,5	84	5	11	0	0,25	0,03
3-5	23,5	77	17	6	0	0,17	0,02
4-3	30	84	0	16	0	0,17	0,02
5-4	40,5	44	10	5	41	40,87	4,9
7-2	57	56	10	13	21	24,69	2,96
9-6	82	58	60	34	0	0,92	0,11
12-3	105	46	6	20	28	30,7	3,69
13-2	132	75	7	18	0	0,25	0,03
18-5	165	83	5	12	0	1,08	0,13
21-3	190	71	9	20	0	0,75	0,09
24-5	220	74	9	17	0	0,5	0,06
27-5	250	76	13	11	0	0,33	0,04
30-3	275	35	19	4	42	46,7	5,6
33-5	308	82	5	2	11	12,76	1,53
36-5	336	90	4	6	0	2,67	0,32
39-5	365	90	8	2	0	0,25	0,03
42-3	391	89	9	2	0	0,25	0,03
45-4	421	87	9	4	0	0,33	0,04
48-3	448	89	8	3	0	0,33	0,04
HOLE 675							
2-2	325	77	3	20	0	0,42	0,05
3-2	334	80	9	11	0	0,17	0,02
4-3	345	80	14	6	0	0,25	0,03
5-3	355	89	4	7	0	0,42	0,05
6-5	366	76	8	16	0	0,17	0,02
8-4	385	80	14	6	0	0,08	0,01
HOLE 676							
1-3	5	45	15	16	24	29,44	3,53
2-5	13	31	8	35	26	29,77	3,57
3-5	22	46	9	6	39	40,87	4,9
4-5	33	49	16	11	24	21,52	2,58
5-5	42	51	13	32	4	4	0,48
7-5	61	55	11	8	26	23,44	3,53
8-5	70	41	14	3	42	35,95	4,31
10-5	89	46	10	3	41	40,53	4,86
12-2	105	51	6	11	32	53,7	4,28
15-2	133	54	13	8	25	26,52	3,18
17-5	155	73	10	5	12	16,68	2
19-5	170	82	10	8	0	0,25	0,03
21-5	190	82	12	6	0	0,67	0,08
23-4	210	84	7	9	0	0,25	0,03
25-1	228	71	12	13	4	3,84	0,46
27-5	250	0	80	20	0	0,25	0,03
28-6	260	76	7	17	0	0,5	0,06
30-5	275	81	16	23	0	0,25	0,03
31-3	286	45	26	29	0	0,33	0,04
32-3	295	70	10	20	0	0,33	0,04
33-5	305	67	21	12	0	0,17	0,02

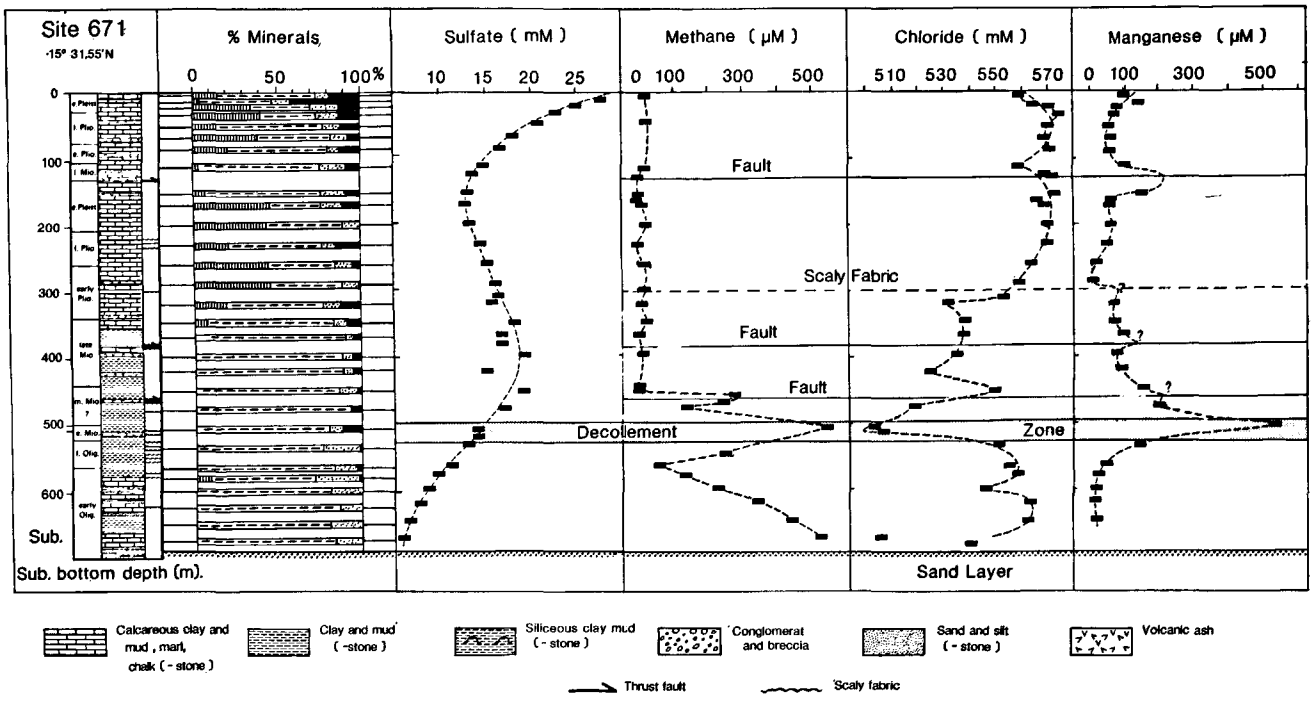

Figure 3

From left to right: age; lithology; structure; percentage of minerals:
calcite, ▥ total clay, ▭ quartz, ▩ plagioclase ■ ; Concentration-depth profile of sulphate, methane, chloride, manganese; site 671.
De gauche à droite : série biostratigraphique ; lithologie ; structure tectonique : pourcentages des composés minéralogiques majeurs :
calcite, ▥ argiles, ▭ quartz, ▩ plagioclase ■ ; profils de concentrations en sulfate, méthane, chlorure, manganèse ; site 671.

ranging between 3 and 35 µM. Below, we notice three maxima in the methane concentrations.

- At 458 and 470 mbsf, the methane concentrations determined are respectively 286 and 258,2 µM. These high methane concentrations correlate with the reverse thrust at 467 mbsf.
- The highest methane measured in this hole (about 550 µM) occurs at the *décollement.*
- From 540 to 570 mbsf, the intensity of the developed scaly fabric of the *décollement* dies out with depth. In this interval, the concentrations of dissolved methane and manganese decrease with depth and the chloride concentration increases. Penetration of an unstable Eocene sand layer halted drilling before the oceanic crust was reached. Unfortunately, we were unable to determine the methane contents in this sand layer at the bottom of Hole 671. However, the last six methane concentrations measured show a quite linear increase with depth. Extrapolation of this trend toward the deeper sand horizon suggests that methane concentrations in the underlying sand layer reach values at least comparable to that found in the *décollement.* In most open ocean drill sites dissolved chloride concentrations are nearly constant with depth, which reflects the relatively small variations in the dissolved chloride concentrations of the world during the last few hundred million years (Gieskes, 1975, 1983).

However, at Site 671 the concentration-depth profiles indicate that the lowest dissolved chloride concentration (505 mM) occurs in the *décollement* zone and this low chloride concentration is associated with a maximum of dissolved methane (550 µM) and manganese (535 µM). The high values of manganese concentrations measured between 100 and 150 mbsf could also be related to a low-angle reverse fault with a throw of 130 m. The occurence of this fault is strongly suggested by a biostratigraphic inversion of upper Miocene over lower Pleistocene sediments observed at 128 mbsf. At this depth, there is a decrease of chloride concentration and no methane concentration anomaly is found. Both above and below the *décollement*, gradients of gradually increasing chloride and decreasing manganese concentrations occur, with the upward manganese gradient being much steeper than the chloride gradient.

Site 675

At site 675, cores were obtained only between 320 and 385 mbsf. In this interval, distinct maxima of dissolved methane (about 724 µM) and manganese (about 524 µM) associated with a distinct minimum in chloride (about 500 mM) were found at 325 mbsf (Fig. 4). At these level, the presence of a fracture zone is indicated by a scaly fabric development at this depth.

Below 360 mbsf, the high manganese and methane concentrations (517 and 394 µM respectivelly) are found in the *décollement* also represented in this site by an interval of interlayered orange-brown radiolarian-bearing

mudstone and olive to olive-brown non-siliceous to siliceous mudstones from the early Miocene. However, chloride concentrations show strong variability in this horizon.

Site 672

Site 672 was intended as a reference hole the Leg 110 transect and was located six kilometres off the toe of the accretionary prism. The concentration depth-profiles for methane, chloride, and manganese are shown in Figure 5.

The most important result shown in these profiles is the high methane and manganese concentrations in the radiolarian rich sediments at the depth range of 180-220 mbsf. As at Site 675, dissolved chloride concentrations show strong variability with, therefore, a significant low chloride concentration at the bottom of this interval. The lithology and age of this horizon are identical to the stratigraphic horizon along which the *décollement* develops at Site 671.

Structural features, such as mud-filled veins, low-and high-angle shear zones, suggest that the stress regime of the encroaching accretionary wedge apparently propagates at least six kilometres seaward from the deformation front to Site 672. This lower Miocene section also has higher bulk porosity with respect to the surrounding sediment, probably related to its high radiolarian content. Such high porosity at this level in Hole 672 can also indicate an abnormal fluid pressure in this less compactible bed, hence facilitating localized failure (Mascle, Moore *et al.*, 1988).

Above the *décollement*, the sedimentarty sequence consists of 110 metres of calcareous clay and mud, marl, and frequent ash layers in a lower Pleistocene to Pliocene section and 55 m of late Miocene mudstone with local ash layers. In accordance with the lithological observation, the semi-quantitative diffraction analysis indicates abundance of calcite in the Pleistocene and Pliocene sections and that, however, the most abundant mineralogical constituents in late Miocene section are clay minerals. From the sea floor to the future *décollement*, note that methane concentrations are higher than those measured above the décollement at Site 671.

Below the *décollement*, penetration of 105 metres of Oligocene interbedded claystone, calcareous claystone and mudstone, marl and thin silt layers, was achieved. The middle to upper Eocene sandy interval which stopped drilling at Site 671 was completely penetrated at the reference site. The Eocene section is formed of calcareous mudstone and marl, micritic limestone, and calcarenite and glauconitic sand. In these sedimentary sequences, we notice two maxima of the methane concentration which are related to the quartz-rich horizons, well defined by the semi-quantitative diffraction analyses at 346 and 424 mbsf.

However, the large sandy layer described by the lithological observations at the top of the middle Eocene sequence is not characterized by a large amount of quartz in the sample used for geochemical studies (Fig. 5). Note that the lowest methane concentration was measured at this level. Below 274 mbsf, the trend of the methane and manganese concentrations is toward increase with increasing depth. Below the *décollement*, the concentration-depth profile of dissolved chloride shows remarkable complexity, with chloride extrema occuring at various depths in the sedimentary column.

Site 676

Site 676 is located on the lower slope, 250 m arcward from the deformation front. The main aim of this drilling site was to document the present structural and hydrological processes at the toe of the accretionary complex. The lithology and mineralogy of this site are given in Figure 6.

The early Pleistocene to upper late Miocene sequence consists of calcareous mudstones and claystones, well documented by the high calcite percentages, and interbedded ash layers well characterized by the enhanced plagiolcase percentages. Between 168 and 263 mbsf, late Miocene sediments are essentially composed of claystones and mudstones, as shown by the elevated amounts of total clays. At 250 mbsf, the high quartz amount suggest the occurence of a thin sandstone layer. From 263 to 310 mbsf, the deepest lithological unit comprises claystones, siliceous mudstone and ash layers. In this lower part, percentages of quartz and plagioclase increase. This unit is early Miocene in age according to its radiolarian content.

Figure 6 gives the dissolved methane, chloride, and manganese concentrations. The plot of the methane concentration versus depth shows three positive anomalous zones which are well correlated with the three compressive structures recording some of the earliest effects of offscraping.

From the bottom to the sea floor, we notice following three chemical zones:

- First, at 386 mbsf, 150 µM of methane has been determined in the interstitial water extracted from the lower Miocene radiolarian-rich sediments sampled at the level of the deepest tectonic zone of this site. In accordance with the seismic correlation from Sites 672 to 671, this shearing zone is interpreted as the oceanward progagating *décollement* (Mascle, Moore *et al.*, 1988). This interpretation is also supported by the observation of tectonic features such as dilatant veining, incipient subhorizontal shearing and associated biostratigraphic inversion at 271 and 305 mbsf. In good agreement with the results obtained at Sites 671 and 675 in the *décollement* and at Site 672 in the propagating *décollement* in oceanic domain, the enhanced methane

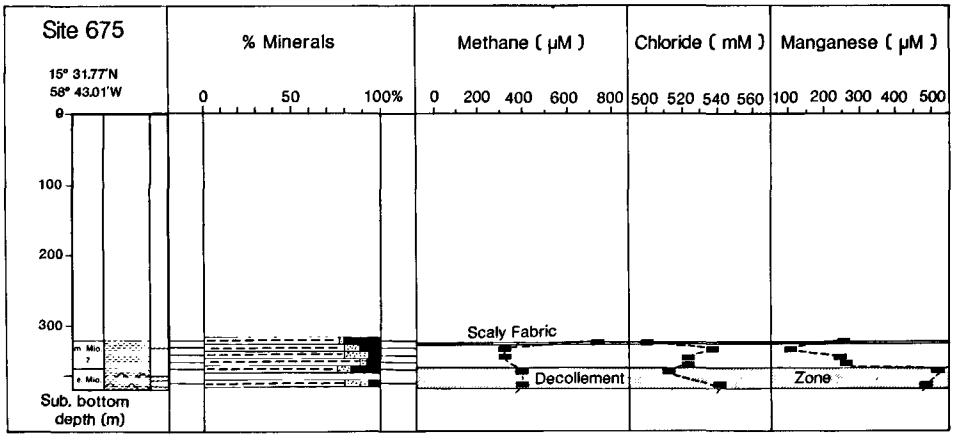

Figure 4

Age ; lithology ; structure ; percentage of minerals ; concentration-depth profiles of methane, chloride and manganese ; site 675.
Série biostratigraphique ; lithologie ; structures tectoniques ; pourcentages des composés minéralogiques majeurs ; profils de concentrations en méthane, chlorure, manganèse ; site 675.

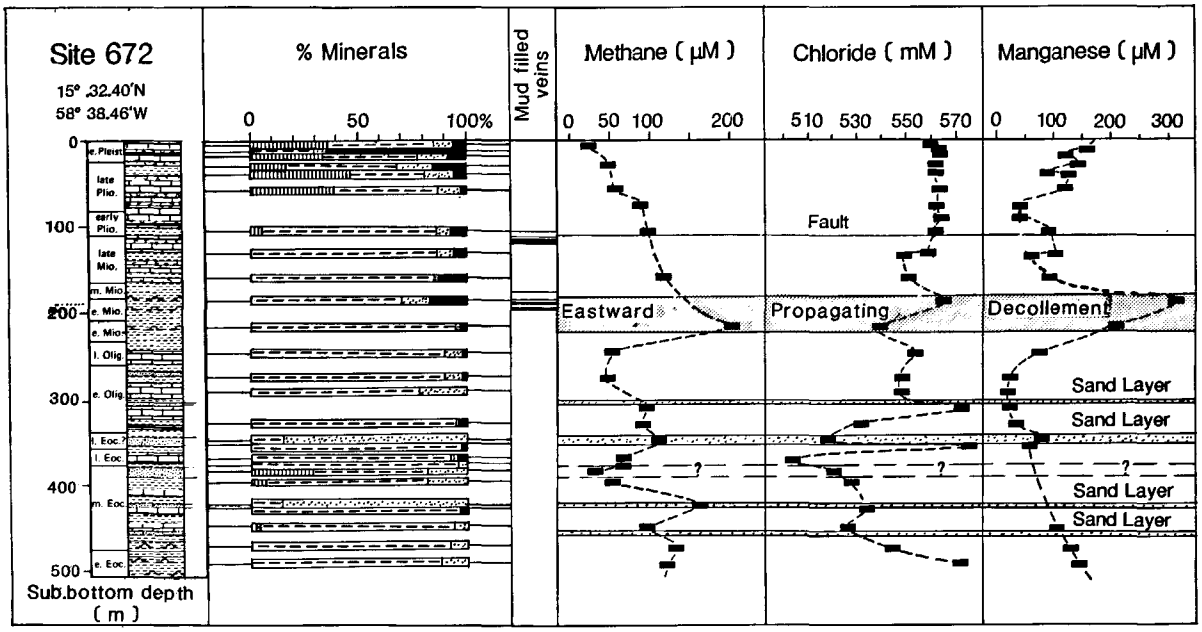

Figure 5

Age; lithology; structure; percentage of minerals; occurrences of mud-filled veins; concentration-depth profile of methane, chloride and manganese; site 672.
Série biostratigraphique ; lithologie ; structures tectoniques ; pourcentages des composés minéralogiques majeurs ; profils de concentrations en méthane, chlorure, manganèse ; site 672.

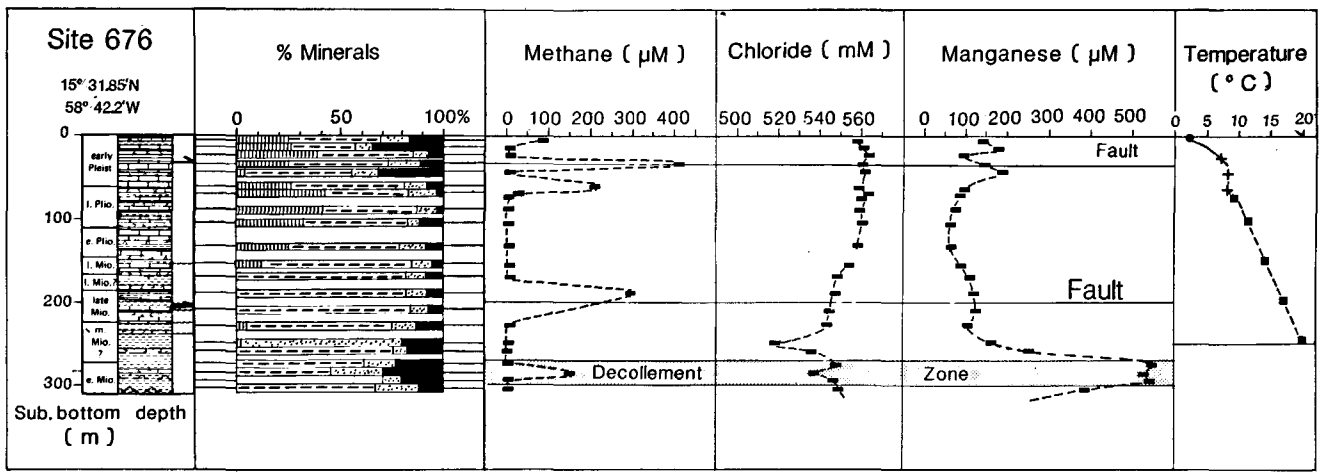

Figure 6

Age ; lithology ; structure ; percentage of minerals ; concentration-depth profiles of methane, chloride and manganese ; site 676.
Geothermal gradient profile ; site 676. ● ----- + : 60°C/km; + --------- + : 92°C/km ■ ------- ■ : 186 °C/km (*Mascle* , Moore et al., *1988)*
Série biostratigraphique ; lithologie ; structures tectoniques ; pourcentages des composés minéralogiques majeurs ; profils de concentrations en méthane, chlorure, manganèse ; site 676.
Profil du gradient de température en fonction de la profondeur ;
site 676 : ● ------ + : 60°C/km ;+ --------- + : 92°C/km ■ ------- ■ : 186°C/km (Mascle, Moore *et al.*, 1988).

concentration observed at this level in Hole 676 is associated with a characteristic manganese anomaly with concentrations in the 528 to 544 µM range and a less significant chloride anomaly, about 537 mM.

- Second, the methane anomaly determined at Hole 676 a concentration of about 293 µM at 190 mbsf and can be related to a biostratigraphically defined thrust fault and an associated zone of scaly fabric at 210 mbsf which repeats an upper Miocene interval about 30 m thick. This fault apparently represents a newly propagating frontal thrust (Mascle, Moore *et al.*, 1988). Note that this high methane content is also associated with some enhanced manganese concentrations. The lowest chloride concentration of this hole occurs, at 250 mbsf, in an X-ray defined thin sandstone layer interbedded in clay rich sediments, and is not correlated with methane and manganese anomalies.
- Third, the methane anomalous zone is closely related to a tight folding of Pleistocene sediments and a small-scale reverse fault at about 30 mbsf, probably representing the shallowest expression of the frontal thrust of the acrretionary front. Maximum methane concentrations, reaching 409 and 206 µM at 33 and 61 mbsf respectively, are associated with a peak of manganese, 187 µM at 42 mbsf. These positive anomalies are not associated with a negative chloride anomaly. These geochemical data are also related to the sediment temperatures measured during Leg 110 (Mascle, Moore *et al.*, 1988).

Sites 673 and 674

Sites 673 and 674 were drilled 12 and 17 km up slope and west of the deformation front to measure the continuing deformation in the accreted sediments during their progressive uplift. There is a significant change in geochemical observations as well as in the stratigraphy of the accreted section and the deformation style obtained with the transect of Sites 676, 675 and 671. Sediments are much more deformed than near the deformation front. However, their porosity of about 50 % indicates that the potential for fluid expulsion will still be significant during continued structural evolution (Moore, Mascle *et al.*, 1988). The sites are located in an area of a significant slope apron that includes resedimented material derived from up slope.

Site 674

Site 674 was drilled in the westernmost area of the drill transect, 17 km arcward from the deformation front. The hole penetrated 452 m of sediments ranging in age from middle Eocene to early Pleistone. Thus, stratigraphic units of Oligocene and Eocene age, observed below the incipient *décollement* zone at Site 672, occur in the upper part of the sedimentary column at Site 674. This suggests that during the accretion of these tectono-stratigraphic packages the basal *décollement* was located in very much older sediments (Mascle, Moore *et al.*, 1988). Sediments at this site consist of large heterogeneous lithological sequences (Fig. 7). They are essentially composed of calcareous, and siliceous mudstone, claystone, and marl with few ash and sandstone layers. Also interbedded chalk, limestone, and calcareous mudstone occur in the middle Eocene section, as documented by high amounts of calcite determined by X-ray diffraction analysis in this interval. Structural features, such as overturned sections, scaly fabric, stratal disruption, abundant calcite veins, and cataclastic shear zones indicate the occurence of many fractures zones. Concentration-depth profiles of chloride and manganese in the upper 30 mbsf show a clearly established chloride minimum associated with a sharp manganese maximum.

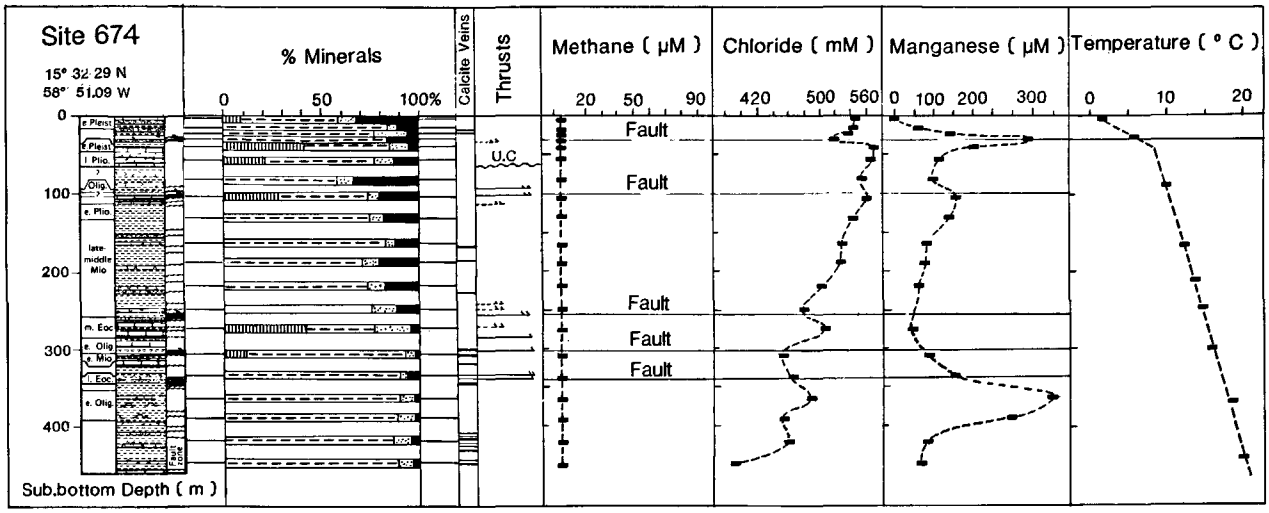

Figure 7

Age; lithology; structure; percentage of minerals; occurrences of calcite veins; concentration-depth-profile of methane, chloride and manganese; site 674.

Geothermal gradient profile; site 676 (Mascle, 1988)

Série biostratigraphique ; lithologie ; structures tectoniques ; pourcentages des composés minéralogiques majeurs ; profils de concentrations en méthane, chlorure, manganèse ; site 674.

Profil du gradient de température en fonction de la profondeur ; site 674 (Mascle *et al.*, 1988).

From 30 to 250 mbsf, the manganese concentration decreases with increasing depth. We notice a manganese anomaly reaching a maximum concentration about 152 µM at 105 mbsf. This manganese anomaly is probably related to a structurally well defined thrust fault occuring at 100 mbsf.
Below 40,5 mbsf, the chloride concentration profile shows a decrease with increasing depth. In inference to Site 671, this very steep chloride concentration-gradient could be related to an diffusion exchange between a very low concentration level in the *décollement* (probably located below 1 000 mbsf at Site 674) and high chloride concentrations at the top the Hole 674.
Below 250 mbsf, the highest manganese concentration, about 397 µM at 365 mbsf, is determined in the brown radiolarian-bearing claystone of Oligocene age and is not related to any potential thrust faults. Negative chloride anomalies are related only to some of the structurally documented faults and are not associated with manganese anomalies.

Site 673

Site 673, which is positioned some 12 km west of the toe of the accretionary prism, involved 331 m penetration in Hole 673B. The cored section at this site is subdivided into two lithological units (Fig. 8).
The first, about 75 m long, consists of calcareous muds and marls of Pleistocene and Pliocene age. Lithological facies, such as debris flow deposits and bedded marls are seen to be of a slope sediment origin.
The second lithological unit, extending from 75 to 331 m, consists of middle and lower Miocene claystones and siliceous claystones. X-ray diffraction analyses show the occurence of calcite in the upper and indicate that clays predominante in the lower unit.

The concentration-depth profiles of the dissolved methane, chloride and manganese are shown in Figure 8. Dissolved chloride and manganese concentrations show quite similar variability versus depth.
Below 50 mbsf, chloride and manganese concentrations decrease with depth. However, an especially steep chloride gradient occurs between 105 and 136 mbsf and dissolved chloride reaches steep chloride gradient occurs between 105 and 135 mbsf and dissolved chloride reaches relatively constant concentrations ranging from 513 to 505 mM between 136 and 200 mbsf in the overturned lower limb of an anticlinal fold, probably caused by thrusting along a scaly fabric zone about 20 m thick. The base of this fold, consisting of carbonate-free claystones, is characterized by calcite filled veins (Mascle, Moore *et al.*, 1988).
Below 200 mbsf, maxima of about 543 mM and 522 µM, for chloride and manganese respectively, occur between 230 and 260 mbsf. At 290 mbsf, the dissolved chloride and manganese concentrations shows sharp minima of about 491 mM and 182 µM respectively, followed by a large increase of these elementary concentrations at the bottom of the hole.
Note that the highest manganese concentration determined at Site 673 occurs in the orange-brown radiolarian-rich claystones of the biostratigraphically equal level of the *décollement* zone and reaches amounts comparable to those determined in the *décollement* at Sites 671, 675 and 676.

DISCUSSION

One of the major results of the Leg 110 programme on board the Joïdes Resolution has been to apply a chemical characterization of the *décollement* zone, the future

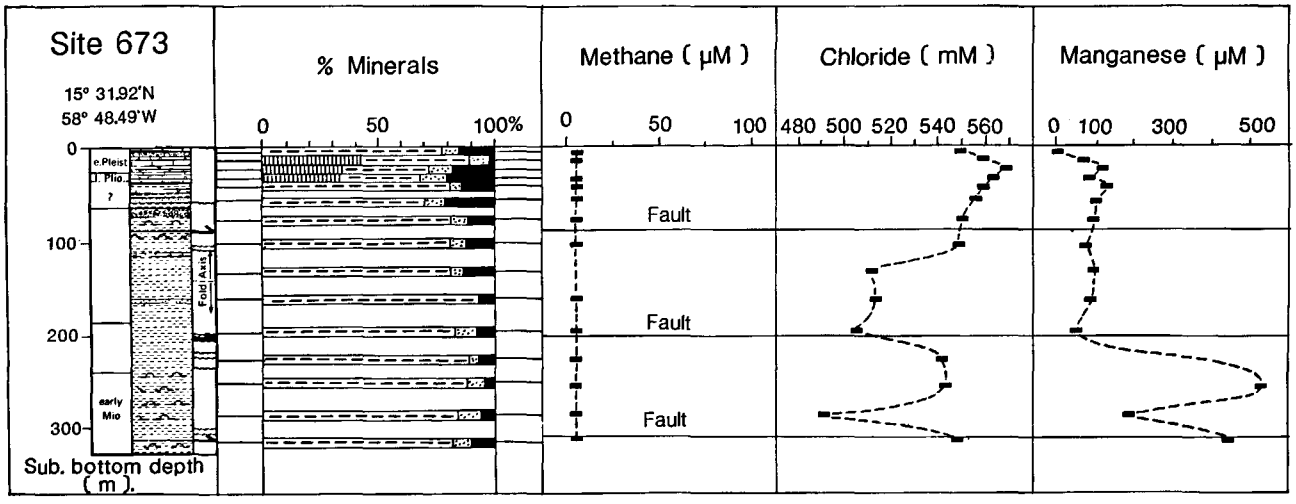

Figure 8

Age; lithology; structure; percentage of minerals; concentration-depth profiles of methane, chloride and manganese; site 673.
Série biostratigraphique : lithologie ; structures tectoniques ; pourcentages des composés minéralogiques majeurs ; profils de concentrations en sulfate, méthane, chlorure, manganèse ; site 673.

décollement zone and also thrusting faults associated with these basal detachment surfaces. We saw that these main structures of the northern Barbados accretionary prism are clearly characterized by positive methane and manganese anomalies associated with more or less negative chloride anomalies.

The origin of the dissolved methane in the interstitial waters of the sediments cored during Leg 110 improves the hypothesis of advection of fluids along the *décollement* and more permeable zones of the northern Barbados accretionary complex. Methane can be produced in nature by both microbial and thermal degradation of organic matter. At Sites 671, 675, 676 and 672, the high methane contents determined in interstitial waters containing dissolved sulphate suggest that the methane sampled is not biogenically derived. Indeed, there is some evidence that methane is not produced in sediments until dissolved sulfate is nearly or totally removed by sulfate reducing-bacteria (Nissenbaun *et al.*, 1972; Claypool and Kaplan, 1974; Martens and Berner, 1977). On the other hand, the lack of methane observed at sites 673 and 674 below the sulphate reduction zone also indicates that no biological methane production occurs in this site (Gieskes, Blanc *et al.*, 1989). $C_1/(C_2 + C_3)$ ratios measured in the interstitial water samples taken from Hole 676 range from 1 to 3 and consequently indicate a relatively high production of C_2 and C_3 light hydrocarbons.

Determinations of carbon isotopic ratio of gas samples taken from the *décollement* zones at sites 671, 675 and 676 indicate that the $\partial^{13}C$ of the methane is probably around 38 ‰ (*vs.* PDB; Gieskes *et al.*, 1989). Both the very low $C_1/(C_2 + C_3)$ ratios and the characteristic isotopic composition of methane strongly suggest a thermogenic methane production (Schoell, 1983; 1984). Also, the $C_1/(C_2 + C_3)$ ratios measured in the water from the events in the Nankaï trough and Japan trench suggest a thermogenic origin of methane in these subducting environments (Boulègue *et al.*, 1987 *a, b*).

The thermogenic light hydrocarbon production in the sedimentary series occurs at temperatures higher than 50-60°C. At the depths of occurrence of methane at sites 671, 675, 676, and 672, temperatures are not high enough for thermogenic methane to form *in situ*. Hence, we postulate that the thermogenic methane has its origin at much greater depths than that reached at site 671 and, consequently, this indicates a deep source for the fluid sampled in the *décollement* and associated faults and, also, in the underlying permeable sand layers. In this case, positive methane anomalies observed in sites 671, 675, 676, and 672 result essentially from methane-rich fluid circulation along the *décollement* and from its propagating in the oceanic domain and along the reverse faults characterizing the present deformation front of the northern Barbados accretionary wedge. Sand layers encountered below the *décollement* at sites 671 and 672 probably act as additional drainage zones.

The sediments temperatures measured during Leg 110 (Mascle *et al.*, 1988) well improve an advection of fluid along major tectonic pathways. In comparison the thermal regime predicted by cooling plate models (Anderson and Skilbeck, 1982; Lister, 1977) and thermal models of active margins (Hsui and Toksoz, 1979), all the site 676 thermal gradients are anomalous (Fig. 6). A gradient of 60°C/km is more than twice that predicted by either type of model. An explanation of these anomalous gradients might be that warm fluid is flowing along a frontal thrust and raising sediment temperatures both below and above this conduit. Similar anomalous temperatures have been explained by fluid flow in the subducting area off Japan (Boulègue *et al.*, 1987, a, b). In accordance with these observations, the high concentrations of manganese and methane determined just beneath the sea floor strongly suggest venting of warm fluid in the vicinity of the toe of the prism at site 676.

In the same way, the clearcut anomaly in thermal gradient described at 30 mbsf at site 674 (Mascle *et al.*, 1988) strongly supports the concepts that the low chloride and enhanced manganese concentrations determined at this level are of recent origin, resulting in an unsteady state both in these elements and in the temperature distributions. These significant results can be understood best in terms of advection of warmer sedimentary fluids from greater depth along a potential landward-dipping faults. We notice that advected low-chloride and high-manganese containing water does not appear to carry any significant amount of methane. If methane anomalies strongly suggest fluid advection along major thrust faults, characteristic observations have been noted on the methane concentration-depth profiles:

- no methane anomaly occurs at sites 673 and 674;
- at sites 671, 675 and 676, methane anomalies are mainly restricted to zones of potential lateral advection;
- at site 672, methane concentrations above the future *décollement* are higher than those measured on either side of *décollement* and major thrust faults of the sites 671, 675 and 676.

We suggest that the lowest methane concentrations can be best understood in terms of diagenetic processes. In spite of sulphate reducers that greatly prefer organic compounds other than methane as sources of energy, it is generally assumed in subsurface sediments that methane diffusing upward from the source can be consumed by sulphate-reducing bacteria and associated micro-organisms in the zone in the zone of sulphate reduction (Barnes and Goldberg, 1976; Martens and Berner, 1977; Berner, 1980). Furthermore, the bacterial metabolism continues, even after burial under as much as 800 m of sediments and in pore waters that have been buried for times in the order of ten million years (Claypool and Kaplan, 1974). Thus the reaction of methane with sulphate:

$$CH_4 + SO_4^{--} \text{-----} > HS^- + HCO_3^- + H_2O$$

could be favoured under conditions found in sedimentary column of sites 676, 671, 673 and 674.

In site 671 from 300 to 458 mbsf, sulphate concentrations show great variability with a slight minimum of about 15 mM at 420 mbsf (Gieskes *et al.*, 1989) which could result from a consumption of SO_4^{--} with respect to higher surrounding concentrations. Hydrogen sulphide has not been detected in the interstitial waters. However, pyrite encountered in the whole sedimentary column may be related to production and consumption of HS^-. Below the *décollement* sulphate reduction continues to be important and methane consumption probably occurs at 566 mbsf. Then, in the deeper part of the hole 671, sulfate comes to zero while methane increases. Hence, methane is probably not consumed below the sulfate reduction zone. Thus could be explained the difference of methane concentrations between, above and below the *décollement.*

In site 676, the sulphate concentrations range from 26 to 15 mM (Gieskes *et al.*, 1989), and pyrite has been observed in the whole sedimentary column, (Mascle *et al.*, 1988) also suggesting a plausible consumption of methane by bacteria in the sediments on either side of thrust faults.

In sites 673 and 674, the methane concentrations below the detection limit of the used determination method can also be related to a methane consumption at greater depth, and for a longer time than that inferred for the other sites.

In site 672, from the seafloor to the future *décollement*, SO_4^{--} concentrations range between 30 to 20 mM (Gieskes *et al.*, 1989), but pyrite is not observed (Mascle *et al.*, 1988). This result suggests that no methane consumption occurs in this zone. Even if pyrite is not observed, however, we shall see in the subsequent section that we cannot rule out the possibility that a methane concumption exists via a reduction of the iron and manganese oxihydroxides observed in this interval. In the second case, the methane concentration determined at the top of the propagating *décollement* could be much higher than methane concentration determined at the bottom of the propagating *décollement.* Furthermore, the difference of methane concentration above the *décollement* between Sites 671 and 672 could be best understood in terms of upward advection of dissolved methane from the *décollement* interval to the sea floor. The high density of tectonic veins at the top of the *décollement* and at 150 mbsf, and the high porosity determined from 0 to 200 mbsf (Mascle *et al.*, 1988) probably help an upward methane escaping at site 672.

The next problem is to explain the occurrence of high manganese concentrations. From sites 671 to 672, the maxima of manganese concentrations occur in the orange-brown radiolarian-rich claystone of the *décollement* zone. Note that manganese-iron oxihydroxides were found in the *décollement* interval. The increase of the manganese concentration of pore water is generally understood in terms of oxidation of organic carbon and reduction of solid manganese dioxide occurring in sediments. A generalized hypothetical reaction is:

$$H_2O + CH_2O + 2\,MnO_2 \longrightarrow 2\,Mn^{2+} + HCO_3^- + 3\,OH^-$$

As the organic carbon contents are very low (< 0.2 %) in the whole sediments (Mascle *et al*, 1988), we postulate that a partial oxidation of methane circulating along the *décollement* zone caused the reduction of some of the manganese oxides observed. This hypothesis is effectively supported by the observations made at Site 675. At this site, indeed, the methane concentration in the *décollement* is lower than that determined at this level at site 671 and abundant manganese oxide and manganese micronodules have been found. Furthermore, the occurrence of rhodocrosite in the *décollement* at site 675 (Mascle *et al*, 1988) suggests that the manganese concentration of interstitial waters represents a saturation value with respect to this mineral. A plausible chemical equilibrium is:

$$Mn^{2+} + HCO_3^- + H_2O \longrightarrow MnCO_3\,(\text{precipitate}) + H_3O^+$$

However, manganese oxides are not systematically found in the fracture zones; sometimes pyrite occurs. Thus, manganese anomalies measured at the fault levels can be best understood if we consider both reduction of manganese oxide by reaction with dissolved methane and advection of dissolved manganese-rich fluid produced in the *décollement* or other horizons in which reduction of manganese can be effective. In both cases, the oxidation of methane by reactions with dissolved sulphate and solid manganese dioxide may explain why manganese anomalies are not always time-associated with methane anomalies at the faults penetrated in the offscraped series at site 671 and in the shallowest fault at site 674. At sites 673 and 674, manganese-iron oxihydroxides have been encountered in the whole sedimentary column and the highest manganese concentrations occur in the characteristic orange-brown radiolarian-rich claystone of early Miocene and Oligocene age respectively. While no active thrust fault was documented at these levels, we propose that these horizons acted as major pathways in the past and could be related to a remnant of fossil *décollement* zones.

We shall now discuss the concentration-depth profiles of the dissolved chloride in the interstitial waters. In all sites, the dissolved chloride concentrations show great variability *versus* depth. However, three major trends characterize these profiles.

- First, chloride concentrations show a progressive freshening of the interstitial water column toward the west on to the accretionary complex. This first characterization of the chloride profiles is apparently related to the increasing pressure in response to the thickening of the sedimentary series toward the west.
- Second, concentration-depth profiles show large variations of chloride concentrations over a short distance. The greatest variations are related to the occurrence of both intense scaly fabric developments and important lithological contrasts. Basically, this second trend is derived from a local phenomenon causing a great change in chloride contents over a short distance.

• Third, low chloride concentrations are related to some of the major tectonic structures such as the *décollement* zone at sites 671 and 675, eastward propagating *décollement* at sites 676 and 672, reverse thrusts associated with these detachment surfaces, and also probably to the sand layers occurring in the underthrust sedimentary series. These negative chloride anomalies are associated with positive methane and manganese anomalies and also sometimes with well defined positive temperature anomalies such as these observed at sites 676 and 674. Hence, this third characterization of the concentration-depth profiles of chloride can be best understood in terms of advection of low chloride fluids from a deeper source into the accretionary complex.

The next problem is to define the potential processes leading to the changes of the dissolved chloride concentrations of the interstitial waters. Previous studies of interstitial waters in accretionary prisms in the area of the middle America trench during DSDP Legs 66, 67 and 84 have revealed large decreases in the concentrations of dissolved chloride (Harrison *et al.*, 1982; Hesse *et al.*, 1985; Gieskes *et al.*, 1985). In these settings, however, the decreases observed in chloride were accompanied by increases in the $\partial^{18}O$ (H_2O) of the interstitial waters and could be considered to be artefacts caused by the decomposition of methane-hydrates during retrieval of the cores. Typically, large amounts of methane-hydrates were recovered during these DSDP legs, and methane gas concentrations were high enough (*i. e.* above 50 mM) to be well into the stability field of methane-hydrates (Claypool and Kaplan, 1974; Hand *et al.*, 1974; Miller, 1974). In Leg 110 sites, however, methane concentrations were always less than 1 mM, and no bottom simulating reflector has been recognized in the Leg 110 seismic lines. This is an indication that the low chloride concentration are not caused by the decomposition of methane-hydrates during retrieval of the cores. However, measurements of the oxygen isotope composition of the interstitial waters suggest an increase of the $\partial^{18}O$ in the *décollement* (Gieskes *et al.*, 1990). So, we cannot rule out the possibility that both high methane and low chloride concentrations result from the same processes as the decomposition of methane-hydrates. Indeed, hydrate decomposition leads, first, to increases $\partial^{18}O$ (H_2O) as a result of the dissolution of ice, second, to dilute the pore water, and third, to remove dissolved methane. Furthermore, the anomalous fluids found at the reference site and at shallow depth in the sedimentary series suggest that these fluids circulated during a sufficiently short period to keep a large portion of their deeper chemical and temperature characteristics. However, the beginning of the thermogenic methane production requires a sufficiently deep origin zone to reach a temperature higher than 60°C. The map of depth to the Atlantic oceanic basement (Westbrook *et al.*, 1984) suggests a great deepening of the sedimentary series toward the south of the Leg 110 transect. In this southern part, hydrate layers are identified on the seismic lines (Griboulard *et al*, 1990), low chloride fluid levels are detected in the subsurface pore water in the vicinity of the deformation front (Griboulard *et al.*, 1989; Fouchet *et al.*, 1990), and a mud volcano has been recognised by the submersible *Nautile* over the deformation front (Le Pichon *et al.*, 1990). All these results strongly suggest an intensive fluid expulsion in the southern vicinity of the Leg 110 area. Thus, we propose that a part of the fluid circulating in the sedimentary series of the northern accretionary wedge probably originated to the south of the Leg 110 transect (Fig. 9). In this case, part of the chemical characteristics of the interstitial water sampled during Leg 110 could be derived from the partial *in situ* decomposition of the hydrate layers, caused by warm fluid expulsion along the major tectonic structures, from the depeer southern area to a shallower northern area.

Therefore, this model cannot explain the scatter in chloride concentrations, especially in the site 672, where chlorinity higher than that of the sea water was determined. Membrane filtration processes appear to be an appropriate phenomenon to explain the variability of the chloride concentrations over a short vertical distance. This membrane filtration process can be related to tectonic dewatering, acting both in the underthrust and offscraped sequences. Under the effect of compaction pressure, interstitial water passes from a high pressure zone into a lower pressure zone through sedimentary formation. During this water transfer, ions will be retained preferentially in less permeable formations such as clays, shales, zeolites and kerogen, and relatively fresh water will be released in the most permeable formation (sandstones, fracture zones). Experimental studies on membrane filtration processes were attempted by several authors (Kharaka and Berry, 1973; Kharaka and Smalley, 1976; Haydon and Graf, 1986). These experimental data indicate that chloride and bromide and monovalent cations are retarded with respect to other anions and divalents cations respectively.

Such processes have often been invoked to explain low salinities observed in overpressurized zones sandwiched between sediment layers containing oil field brines (Fertl, 1976; Hanshaw and Coplen, 1973; Fritz and Marine, 1983; Marine and Fritz, 1981).

The rapid change in chlorinity, particulary significant in Eocene and Oligocene sequences at sites 674 and 672, indicates that it may be possible that a sufficient pressure gradient exists to support the local membrane filtration processes even at porosities in excess of 50 %. We noticed that the scatter in chloride concentrations appear to be inferred to zones characterized by intense scaly fabrics development, and by high intensity of calcite veins. Experimental data suggest that a precipitation of authigenic calcite can be induced by hyperfiltration (Fritz and Eady, 1985). If local membrane filtration processes work in the accreted sedimentary series and in the series not yet underthrust, basically this phenomenon must be much more effective at greater depth in the accretionary wedge where total stresses resulting from the arcward

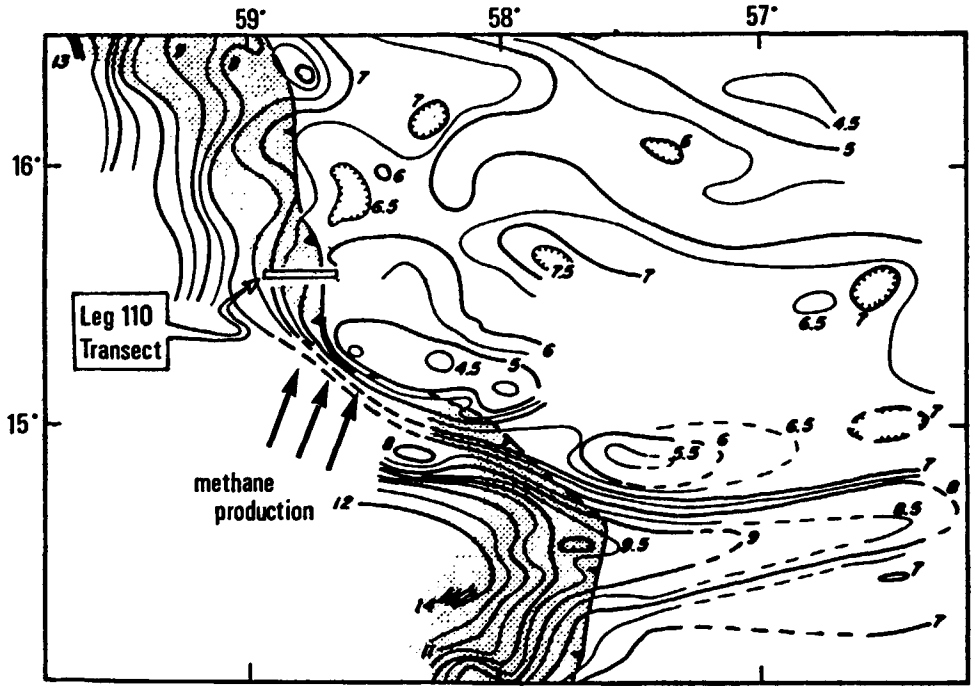

Figure 9

Map of depth in kilometers to the Atlantic oceanic basement derived from seismic reflection data (after Westbrook et al., *1984).*
Carte isobathe du toit de la croûte océanique d'après des données de sismique-réflection (d'après Westbrook *et al.*, 1984).

thickening of the sedimentary series gradually increase toward the west and south. Porosity data (Mascle *et al*, 1988) and methane of thermogenic origin also argue for an expulsion of part of the low chloride fluid produced at

because it involves dehydration of the smectite. Clays determinations suggest that authigenic illite-clay minerals are strikingly poor along the sedimentary column at sites 671 and 672 (Caret *et al*., 1989). Hence

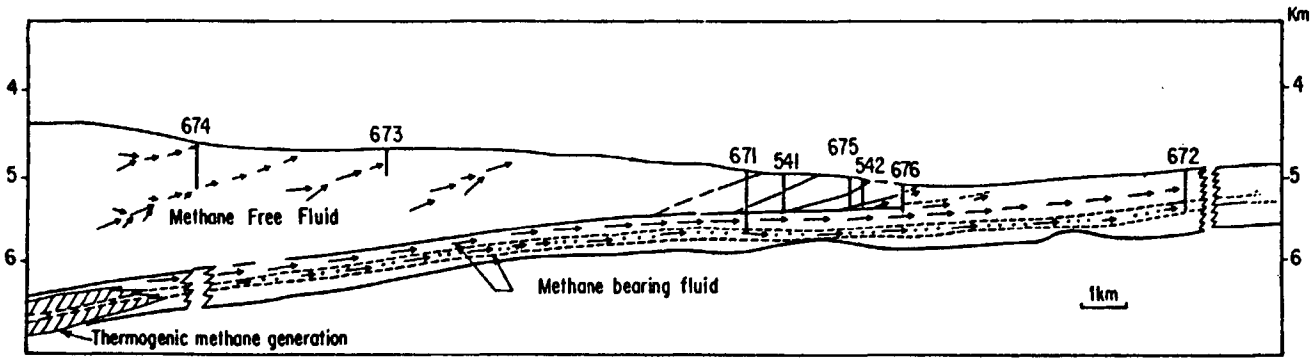

Figure 10

Two-dimensional model of fluid circulation.
Modèle de circulation de fluide en deux dimensions.

• Parts of the fluid go up toward the sea bed at the top of the front reverse faults. However, the maximum value of the dissolved methane concentrations measured during Leg 110 (about 0.6 µM) is largely lower than the quantity of carbon necessary to sustain the growth of clams (Boulègue *et al.*, 1989). Hence, the occurrence of clam fields in the close vicinity of the toe of the prism in place of Leg 110 work zone is unlikely;

• Circulation of methane-rich fluid along the major tectonic structures of the accretionary wedge probably induces the reduction of manganese oxides and consequently removes the manganese as Mn^{2+} in the interstitial water;

• Circulation of fluid with low chloride and high manganese contents, but no accompanying methane, occurs in the offscraped series along tectonic structures enabling the prism to grow from the deformation front. The lack of methane in the upper sedimentary series can be best understood in terms of methane oxidation, probably involving sulphate and manganese oxyde reductions. Thus, diagenetic processes could affect the methane concentrations;

• This oxidation of methane leads to an increase of the ΣCO_2 in the interstitial water and consequently allows the precipitation of calcium and manganese carbonates such as calcite veins described at sites 674 and 673 and rhodocrosite observed in the *décollement* at site 675. Thus, diagenetic processes essentially control the manganese concentrations in the interstitial water of the sedimentary series;

• Positive anomalies in methane and manganese appear to be the more sensitive indicators of fluid flow than the negative anomalies in chloride concentrations which are affected by local membrane filtration processes;

• The hydrogeochemical data obtained during Leg 110 provide a possible two-dimensional model of fluid circulation in subducting environments (Fig. 10). However, it appears to be difficult to determine the zone of origin of these fluids. Therefore, investigations in the southern area of Leg 110 (in the south-west of the Tiburon rise) could probably give some interesting information this question.

• Our observations are of special interest in light of observations made on the venting of hydrocarbon-rich fluids along fault zones in the areas of subduction off Oregon (Kulm *et al.*, 1986 ; Suess *et al.*, 1985) and off Japan (Boulègue *et al.*, 1987 *a, b*). In these areas, it has also been postulated that such fluids may be related to dewatering processes associated with the accretion of thick sediments.

• Methane, manganese and chloride determinations appear to be very effective tools for investigating the relationship between structural, hydrological and diagenetic processes at the toe of an accretionary complex.

Acknowlegments

We are grateful for the support of the ODP Technical, Operations and Engineering groups, and SEDCO personnel who were instrumental in obtaining data reported here. The Ocean Drilling Program is sponsored by the National Science Foundation, the European Science Foundation, and national institutions in Canada, Federal Republic of Germany, France, the United Kingdom, and Japan. Determination of the dissolved manganese contents was performed by Anne-Marie de Kersabiec from the *Laboratoire de Géochimie et Métallogenie* (UA CNRS 196, Paris VI). Determination of the C1/ (C2 +C3) ratios on ten samples was carried out by Jean-Luc Charlou, of the DERO-GM laboratory (IFREMER).

REFERENCES

Anderson R.N. and J.N. Skilbeck (1982). Oceanic heat flow. In: Emiliani C. Ed., The oceanic lithosphere, The Sea, vol. 7, New York, Wiley and Sons, 489-524.

Barnes R.O. and E.D. Goldberg (1976). Methane production and consumption in anoxic marine sediments. *Geology*, **4**, 297-300.

Behrmann J.H., K. Brown and Leg 110 Shipboard Scientific Party. (1988). Evolution of structures and fabrics in the Barbados Accretionary Prism. *Journal of Structural Geology*, **10**, 577-591.

Bernard B.B., J.M. Brooks and W.M. Sackett (1976). Natural gas seepage in the Gulf of Mexico. *Earth Planet. Sci. Lett.*, **31**, 48-54.
Bernard B.B., J.M. Brooks and W.M. Sackett (1978). Light hydrocarbons in recent Texas continental shelf and slope sediments. *J. Geophys. Res.*, **83**, C8, 4053-4061.
Berner R.A. (1980). Early Diagenesis. A theoretical Approach. Princeton Series in Geochemistry. Princeton University Press. p. 241.
Biju-Duval B., J.C. Moore *et al.* (1984). Init. Reports of the Deep Sea Drilling Project, vol. **78**A, p. 621.
Blanc G., J. Boulègue, D. Badaut and P. Stouf (1986). Premiers résultats de la campagne océanographique Hydrotherm (mai 1985) du Marion-Dufresne sur la fosse Atlantis II (mer Rouge). *C. R. Acad. Sci.*, **302**, II, 4, 175-180.
Blanc G. and A.-M. de Kersabiec (1985). Trace metal determinations in pore brines by electrothermal atomic absorption spectrometry with Zeeman effect. 1985 September, Garmisch-Partenkirchen, R.F.G., *Colloquium Spectroscopium Internationale XXIV.*
Blanc G. (1987). Géochimie de la fosse Atlantis II (Mer Rouge). Evolution Spatio-temporelle et rôle de l'hydrothermalisme. Publications de la mission de recherche des TAAF, MD/HYDROTHERM, **85-05**, p. 212.
Blanc G., J.M. Giestres and ODL Leg 110 Scientific Party (1988). Advection de fluides intersticiels dans les séries sédimentaires du complexe d'accrétion de la Barbade (Leg 110 ODP). *Bull. Soc. Géol.*, **8**, 453-460.
Blanc G., J. Boulègue and J.-C. Charlou (1990). Profils d'hydrocarbures légers dans l'eau de mer, les saumures et les eaux interstitielles de la fosse Atlantis II (mer Rouge). Oceanol. Acta, **13**(2), 187-198.
Boulègue J., J.T. Iiyama, J.-C. Charlou and J. Jedwab (1987 *a*). Nankai trough, Japan trench and Kuril Trench: geochemistry of fluids sampled by submersible "Nautile". *Earth Planet. Sci. Lett.*, **83**, 363-375.
Boulègue J., E.L. Benedetti, D. Dron, A. Mariotti and R. Létolle (1987 *b*). Geochemical and biogeochemical observations on the biological communities associated with fluid venting in Nankai trough and Japan trench subduction zones. *Earth Plant. Sci. Lett.*, **83**, 343-355.
Boulègue J., A. Mariotti, P. Cros, C. Rangin and J. Jedwab. Dolomite cement and cementing fluid at 3835 m Depth off Japan. submit to *Chemical Geology.*
Bray C.J. and D.E. Karig (1985). Porosity of sediments in accretionary prisms and some implications for dewatering processes. *J. Geophys. Res.*, **90**, B1, 768-778.
Capet X., C. Beck and H. Chamley (1989). Clay mineral changes in Cenozoic sediments from northern Venezuela and from Barbados ridge accretionary complex. AIPEA, 9th international clay conference, Strasbourg, France.
Claypool G.E. and I.R. Kaplan (1974). The origin and distribution of methane in marine sediments. In: Kaplan I. R. Ed., *Natural Gases in Marine Sediments.* Plenum Press, New York, 99-140.
Fertl W.N. (1976). Abnormal formation pressures: implications to exploration, drilling and oil and gas resources. In: Developments in Petroleum Science, Elsevier Science Publ. B.V., Amsterdam, 190-196.
Fouchet J.-P., X. Le Pichon, S. Lallemant, M. Hobart, P. Henry, M. Benedetti, J. Wesbrook and M. Larent (1990). Heat flow, tectonics and fluid circulation at the toe of the Barbados ridge prism. *J. Geophys. Res.* (in press).
Fritz J.S. and Eady C.D. (1985). Hyperfiltration-induced precipitation of calcite. *Geochim. Cosmochim. Acta*, **49**, 761-768.
Fritz J.S. and I.W. Marine (1983). Experimental support for a predictive osmotic model of clay membranes. *Geochim. Cosmochim. Acta*, **49**, 1515-1522.
Gieskes J.M. (1975). Chemistry of interstitial waters of marine sediments. Annual Revs. *Earth Planet. Sci.*, **3**, 433-453.
Gieskes J.M. (1983). The chemistry of interstitial waters of deep sea sediments: Interpretation of Deep Sea Drilling Data. *Chemical Oceanography*, **8**, 221-269.
Gieskes J.M., K. Johnston and M. Boehm (1985). Appendix. Interstitial water studies, Leg 66. *Init. reports of the DSDP*, 84, 961-967.
Gieskes J.M. and G. Peretsman (1986). Water chemistry procedures on board "Joïdes Resolution" - some comments. *Ocean Drilling Programme, Technical Note*, vol. **5**, p. 46.
Gieskes J.M., G. Blanc and Leg 110 Shipboard Party (1989). Hydrogeochemistry in the Barbados Accretionary Complex: Leg 110 ODP. *Paleo., Paleo., Paleo.*, **71**, 83-96.
Gieskes J.M., P. Vrolijk and G. Blanc. Hydrogeochemistry of the Northern Barbados Accretionary Complex Transect: ODP Leg 110. *J. Geophys. Res.* (in press).
Griboulard R., J.-C. Faugères, G. Blanc, E. Gonthier and G. Vernette (1989). Nouvelles évidences sédimentologiques et géochimiques de l'activité actuelle du prisme Sud Barbade. *C. R. Acad. Sci.*, **308**, II, 75-81.
Griboulard R., C. Bobier, J.-C. Faugères and G. Vernette. Argilokinetic structures within the Strike-Slip of the south leg of the Barbados prism. *Tectonophysics*, (in press).
Hand J.H., D.L. Katz and V.K. Verma (1974). Review of gas hydrates with implications for ocean sediments. In: Kaplan I.R. Ed., *Natural Gases in Marine Sediments.* Plenum Press, New York, pp. 179-194.
Hanshaw B.B. and T.B. Coplen (1973). Ultrafiltration by a compacted clay membrane. II. Sodium ion exclusion at various ionic strengths. *Geochim. Cosmochim. Acta*, **37**, 2311-2327.
Harrison W.E., R. Hesse, and J.M. Gieskes (1982). Relationship between sedimentary facies and interstitial water chemistry of slope, trench and Cocos Plate sites from the Middle America Trench Transcet, DSDP Leg 67. *Init. Reports of the DSDP*, **67**, 603-614.
Haydon P. R. and D.L. Graf (1986). Studies of smectite membrane behavior: Temperature dependence, 20-180°C. *Geochim. Cosmochim. Acta*, **50**, 115-121.
Hesse R., J. Lebel and J.M. Gieskes (1985). Interstitial water chemistry of gas hydrate bearing sections on the Middle America Trench slope, DSDP Leg 84. *Init. Reports of the DSDP*, **84**, 727-737.
Hsui A.T. and M.N. Toksöz (1979). The evolution of thermal structures beneath a subduction zone. *Tectonophysics*, **60**, 43-60.
Huene (von) R. and H. Lee (1983). The possible significance of pore fluid pressures in subduction zones. *Am. Assoc. Petr. Geol. Mem.*, **34**, 791-791.
Jagner D. and K. Aren (1970). A rapid automatic method for the determination of the total halide concentration in sea water by means of a potentiometric titration. *Anal. Chim. Acta*, **52**, 491-502.
Kersabiec (de) A.-M., G. Blanc and M. Pinta (1985). Water analysis by Zeeman Atomic Absorption Spectrometry. *Fresinus Z. Anal. Chem.*, **322**, 731-735.
Kharaka Y. K. and F. A. F. Berry (1973). Simultaneous flow of water and solutes through geological membranes -I. Experimental investigation. *Geochim. Cosmochim. Acta*, **37**, 2577-2603.
Kharaka Y. K. and W. C. Smalley (1976). Flow of water and solutes through compacted clays. *Am. Ass. Petrol. Geolog. Bull.*, **60**, 6, 973-980.
Kulm L.D., E. Suess, T.M. Thornbury, R.W. Embley, D.M. Hussong and J.M. Resig (1986). Fluid venting processes and their relation to tectonic styles in subduction zone of the Eastern Pacific. Abstr. INT. KAIKO conf., 1986; Tokyo and Shimizu, pp. 28-29.
Le Pichon X., J.-P. Fouchet, J. Boulègue, P. Henry, S. Lallemant, M. Benedetti and F. Avedik (1990). Mud volcanoe field seaward of the Barbados accretinnary complex. A submersible survey. *J. geophys. Res.* (in press).
Lister C.R.B. (1977). Estimates for heat flow and deep rock properties based on boundary layer theory. *Tectonophysics*, **41**, 147-171.
Manhein F.T. (1966). A hydraulic squeezer for obtained interstitial waters from consolidated and unconsolidated sediments. *U.S. Geol. Survey Profess. Paper*, **550**-C, p. 256.
Manhein F.T. (1974). Comparative studies on extraction of sediment interstitial waters: discussion and comment on the current state of interstitial water studies. *Clays and Clay Minerals*, **22**, p. 337.
Marine I.W. and Fritz S.J. (1981). Osmotic model to explain anomalous hydraulic heads. *Water Resources Res.*, **17**, 73-82.
Martens C.S. and R.A. Berner (1977). Interstitial water chemistry of anoxic Long Island Sound Sediments - I. Dissolved gases. *Limnol. Oceanog.*, **22**, 10-25.
Mascle A., J.C. Moore and Leg 110 Scientific Party (1988). Proc. ODP, *Init. reports* (part A), **110**, College Station, TX (Ocean Drilling Programme), p. 603.
Miller S.L. (1974). The nature and occurence of clathrates hydrates. In: Kaplan I.R. Ed., *Natural Gases in Marine Sediments.* Plenum Press, New York, pp. 179-194.
Moore J.C., A. Mascle and ODP leg 110 Scientific Party (1987). Expulsion of fluids from along subduction-zone *décollement* horizon. *Nature*, **326**, n° 6115, 785-788.
Moore J.C., A. Mascle and ODP Leg 110 Scientific Party (1988). Tectonics and Hydrogeology of the Northern Barbados Ridge: Result from ODP Leg 110. *Geol. Soc. Am. Bull.*, **100** (10), 1578-1593.
Nissenbaum A.B.J., J. Preslay and I.R. Kaplan (1972). Early diagenesis in a reducing fyord, Sarnich Inlet, British Columbia. - I. Chemical and isotopic changes in major components of interstitial water. *Geochim. Cosmochim. Acta*, **36**, 1007-1027.
Schoell M. (1983). Genetic characterisation of natural gases. *Am. Assoc. Petrol. Geol. Bull.*, **67**(12), 2225-2238.
Schoell M. (1984). Recent advances in petroleum isotope geochemistry. Organic Geochem., Pergamon Press, Oxford, **6**, 645-663.
Suess E., B. Carson, S. Ritger, J.C. Moore, L.D. Kulm and G.R. Cochrane (1985). Biological communities at a vent site along the subduction zone off Oregon. *Biol. Soc. Wash. Bull.*, **6**, 475-484.
Westbrook G.K., A. Mascle and B. Biju-Duval (1984). Geophysics and the structure of the lesser Antilles Forearc. *Init. Reports of the DSDP*, **78**A, 23-38.